

Development and testing of a pyro-driven launcher for harpoon-based comet sample acquisition[☆]

Stefan Völk^{a,*}, Stephan Ulamec^b, Jens Biele^b, Matthias Hecht^a, Peter Lell^c, Josef Fleischmann^a, Sebastian Althapp^a, Markus Grebenstein^d, Joseph A. Nuth^e, Donald C. Wegel^e, Walter F. Smith^e, Lloyd R. Purves^e, Douglas S. Adams^f, Stuart Hill^f, James C. Leary^f, Harold A. Weaver^f, Scott A. Sandford^g

^a German Aerospace Center (DLR), Space Operations and Astronaut Training, Münchener Straße 20, 82234, Weßling, Germany

^b German Aerospace Center (DLR), Space Operations and Astronaut Training, Linder Höhe, 51147, Köln, Germany

^c PyroGlobe GmbH, Hauptstr. 15, 85276, Hettenshausen, Germany

^d German Aerospace Center (DLR), Robotics and Mechatronics, Münchener Straße 20, 82234, Weßling, Germany

^e NASA Goddard Space Flight Center (NASA GSFC), 8800 Greenbelt Rd, Greenbelt, MD, 20771, USA

^f The Johns Hopkins University Applied Physics Laboratory (APL), 11100 Johns Hopkins Rd, Laurel, MD, 20723, USA

^g NASA Ames Research Center (NASA ARC), Moffett Blvd, Mountain View, CA, 94035, USA

ARTICLE INFO

Keywords:

Comet
Sample return
Sample acquisition
New Frontiers
Pyrotechnics
Internal ballistics

ABSTRACT

The CORSAIR (COMet Rendezvous, Sample Acquisition, Investigation, and Return) mission was a proposal for the NASA New Frontiers program. It belongs to the Comet Surface Sample Return mission theme which focuses on acquiring and returning to Earth a macroscopic sample from the surface of a comet nucleus. CORSAIR uses a harpoon-based Sample Acquisition System (SAS) with the spacecraft hovering several meters above the comet surface. This stand-off strategy overcomes disadvantages of other systems such as drills. Since comets are low gravity objects, those techniques would require anchoring before sampling, which is not necessary here. Moreover, the harpoon-based system allows for acquiring several samples from different locations on the comet maximizing the scientific output of the mission.

Each SAS assembly consists of a pyro-driven launcher, a Sample Acquisition and Retrieval Projectile (SARP) and a retraction system using a deployable composite boom structure. In order to collect enough cometary material, the launcher has to provide the required kinetic energy to the SARP. Due to high energy densities, pyrotechnically actuated devices ultimately reduce the overall system mass and dimensions. First, the scientific and technological background of the CORSAIR mission is explained. Then, an overview of the development, design and testing of the launcher is given. Finally, the launcher theory is introduced explaining the entire reaction chain: initiation → gas dynamics → SARP motion.

1. Introduction

Comets are invaluable time capsules that preserve materials from the dawn of the Solar System [1–4]. CORSAIR was one out of twelve proposals submitted to NASA's fourth New Frontiers program [5]. CORSAIR's proposed mission is straightforward: to return to Earth for analysis these early Solar System materials from a comet nucleus [6,7]. Finally, CORSAIR was not one of the two finalist proceeding to Phase A concept studies. This paper describes the proposed mission, the SAS and in particular the launcher subsystem as it was developed during Pre-Phase A over the years

2012–2017. If CORSAIR had been selected, it would have returned the first macroscopic comet samples directly from the nucleus of comet 88P/Howell, as well as coma dust samples. Volatile ices would have been sublimated from the samples and chemically characterized before return. 88P/Howell is ideal for CORSAIR's proposed mission because it is a highly accessible, regularly observed, active Jupiter-family comet that would provide new discoveries from a first exploration.

CORSAIR would have revealed the composition and organic inventory of comets through state-of-the-art analyses of the returned samples. Samples from two distinct surface locations would have been returned to investigate

[☆] This paper was presented during the 68th IAC in Adelaide.

* Corresponding author.

E-mail address: stefan.voelk@dlr.de (S. Völk).

variability across the nucleus. Each nucleus sample would have contained $\geq 45\text{g}$ of material to enable numerous analytical measurements using specialized terrestrial equipment that cannot be easily miniaturized and are far more accurate than their spaceborne counterparts, while also curating $\geq 75\%$ of the sample material for future scientific investigations.

The proposed mission timeline includes launch of the mission on 19 July 2024, rendezvous at comet 88P/Howell from 30 May 2031 to 19 March 2032, and Earth return on 3 July 2036. During rendezvous and monitoring, CORSAIR's payload would have mapped the comet's shape, activity, global morphology, colors, thermal properties, topography, and any changes to these properties over the mission. Coma gas composition and dust flux measurements would have been made continuously during all phases of the comet rendezvous. During four flybys at different sites, images and laser altimetry would have produced local, high-resolution topography maps of potential sampling sites. Subsequently, rehearsals of the descents would have preceded a sampling event. Images would have been acquired before, during, and after each sampling event, to document the sampling process and its effect on the comet's surface. CORSAIR proposes to acquire two nucleus samples from surfaces with diverse properties.

2. Past robotic sample acquisition concepts and designs

Before deciding on a particular implementation of a sample acquisition system, it is essential to compare different concepts and evaluate their advantages and disadvantages. Various systems have been flown in past and current robotic space missions. The missions Genesis [8] and Stardust [9] used a type of passive sample collector. In case of the Stardust mission, a particle collector tray containing blocks of aerogel was exposed to the coma environment of comet 81P/Wild 2 during a flyby of the spacecraft. After sample collection, the collector tray was stowed in a sample return capsule which entered the Earth's atmosphere and landed safely on ground. The particles impacting the aerogel with a relative velocity of 6.1 km/s created long tracks – up to 200 times the length of the grains – and became buried into the silicon-based ultra-high porous material. Although particles larger than $\sim 100\text{ }\mu\text{m}$ were too rare for collection and those smaller than $1\text{ }\mu\text{m}$ were biased by capture effects, the thousands of collected comet particles provided information on outer Solar System materials at a level of detail that probably could never be obtained by remote sensing or in situ methods [10]. A major advantage of the sampling concept is the relatively low mechanic complexity. Furthermore, the concept does not involve landing or near surface operations of the spacecraft. On the other hand, only little sample material from the cometary coma can be acquired.

The Hayabusa 1 and 2 missions use a sampler system consisting of a sampler horn, projectors and a sample storage and transfer mechanism. Upon touchdown of the sampler horn on the asteroid surface, the projector subsystem fires a 4.85 g tantalum projectile on the surface and approximately several hundred milligrams of regolith particles are reflected on the inside surfaces of the sampler horn and stored in a dedicated sample catcher [11]. In order to avoid contamination from propellant combustion gases, a sabot method is adopted for the projectile shooting. A similar sampling technique was presented by Barnouin-Jha et al. in Ref. [12]. Their rock chipper relies on the kinetic energy of a pyrotechnically activated penetrator. The lightweight and recoilless design is suitable for sample generation and collection on planetary surfaces. The penetrator would impact against a rock sample creating a conical sheet of powdered ejecta. The ejecta cone is captured by a catcher which is a ring-shaped container arranged around the penetrator. The firing unit including the penetrator and a gas generating power cartridge is replaced by a robot arm for multiple sampling events. The sampling concepts of the Hayabusa missions and the rock chipper require near surface operations of the spacecraft resulting in higher mission risks and acquire relatively small sample masses. However, the sampling concept is adequate for higher strength materials as expected to be present on asteroid surfaces.

The Touch-And-Go Sample Acquisition Mechanism (TAGSAM) [13] of the launched OSIRIS-REx mission [14] will make use of a burst of nitrogen blowing regolith particles smaller than 2 cm into a sampler

head located at the end of a robotic arm. The concept of operation belongs to a Touch-And-Go strategy limiting the interaction of the spacecraft with the asteroid surface to a few seconds. The system is designed to capture more than 60 g of regolith material. Another sample acquisition concept for a Touch-And-Go mission scenario uses a so-called Brush Wheel Sampler [15] comprising counter-rotating wheels to minimize interaction with the spacecraft, compliant brushes to eliminate jamming and a canister to collect the sample. Due to the Touch-And-Go approach, both concepts minimize near surface operation time. On the other hand, these methods are limited to lower strength or loose surface material such as regolith. The BiBlade concept is another Touch-And-Go sampling device. It overcomes limitations regarding material strength. The high-speed blade penetrator interacts with brittle, porous material [16,17].

A common method for media penetration and sampling is drilling [18,19]. Early examples of robotic space missions equipped with drills are the Soviet programs Luna and Venera [20]. The Luna 16, 20 and 24 landers performed the first fully autonomous drilling on an extraterrestrial body. The Luna landers had a mass of almost 6 tons providing enough inertia for operation of the drill. The drilling mechanism delivered cuttings from a maximum depth of around 2 m . Drills on the Venera landers 13 and 14 penetrated a few centimeters into the subsurface of Venus and retrieved samples for in-situ measurements. Various robotic space missions on Mars are equipped with drills, too. The two Mars Exploration Rovers carry the Rock Abrasion Tool (RAT) [21] which is a grinding tool creating shallow holes in Martian rocks. The Icy Soil Acquisition Device (ISAD) [22] on the Mars 2007 Phoenix Lander included a small cutting bit on a scoop allowing sample acquisition from frozen regolith on arctic plains of Mars. The Mars Science Laboratory (MSL) rover has a drill capable of penetrating a few centimeters into Martian rocks and acquiring powdered samples for further in-situ investigations [23]. Depending on the particular implementation, drills can penetrate deeply into higher strength material. Due to counteracting forces, drill systems are almost exclusively used on celestial bodies with substantial gravity.

An exception of a drill used in an environment with low gravity is the Sampler, Drill and Distribution System (SD2) [24] carried on-board the comet lander Philae. Inter alia, because of balancing counteracting forces during drilling, anchoring of the lander with a harpoon system [25] was planned. However, firing of the harpoons upon touchdown of the lander malfunctioned and Philae bounced several times on the cometary surface until it finally came to rest without being anchored [26]. SD2 is a multifunctional tool designed to penetrate the cometary surface and collect samples at a maximum depth of 23 cm . Before the arrival of the Rosetta [27] mother ship, important environmental conditions of the comet were very poorly known. Particularly, a wide range of possible cometary surface strengths had to be taken into account. Despite the non-nominal landing conditions, SD2 was operated on the comet 67P/Churyumov-Gerasimenko at the end of the primary battery's lifetime. However, no soil samples could be retrieved. An analysis of image data suggests that the distance of the soil from the lander baseplate in the drilling area may have been larger than the maximum offset that can be reached by the drill [28].

A series of studies have been conducted using penetrators for comet surface sampling [29–32]. Penetrators are free flying units which are dispatched by the mother ship and subsequently penetrate the surface of the celestial body. The kinetic energy of a penetrator is gained through the relative velocity of the spacecraft, a launching mechanism or rocket propulsion. No landing of the spacecraft is required, but the spacecraft has to perform near surface operations. Nevertheless, distances to the body surface are larger than in case of most other methods explained above and interaction time is limited. Moreover, several samples from different surface locations can be retrieved. Therefore, the stand-off technique is ideal for these Solar System bodies. Challenges of this method are the imparted momentum if the penetrator is launched from the spacecraft, the correct alignment of the penetrator with respect to the velocity vector and the subsequent retrieval of the sample to the spacecraft.

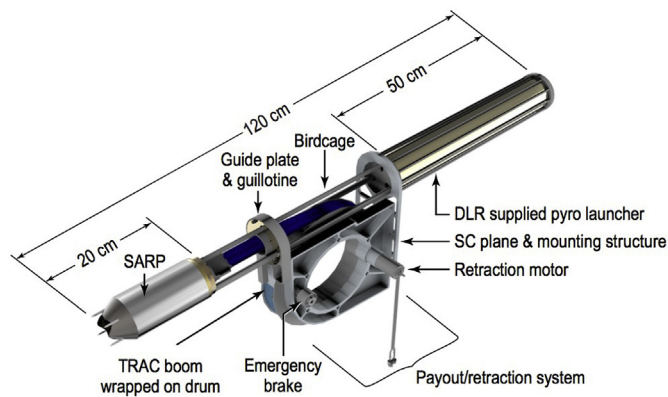


Fig. 1. Assembly of the Sample Acquisition System (SAS) comprising the sub-systems Sample Acquisition and Retrieval Projectile (SARP), retraction system with Triangular Rollable And Collapsible (TRAC) boom and launcher.

3. CORSAIR sample acquisition system

CORSAIR's proposed Sample Acquisition System (SAS) is the culmination of years of studies, hardware development and testing. Sampling was planned to be safely conducted without landing, while the spacecraft would have remained about 10 m above the surface. The SAS is designed to collect material down to depths of at least 10 cm to access more primitive material that may be below the altered surface [6,7]. The system is designed to sample over an extensive range of surface strengths and local topographies, from loose regolith to solid material. Four SAS assemblies each consisting of a pyro-driven launcher, a composite Boom Retraction And Deployment (BRAD) system, and a Sample Acquisition and Retrieval Projectile (SARP) were planned to be installed on the spacecraft. Fig. 1 shows one entire assembly. Each SAS is a self-contained and independently operated unit.

The BRAD is shown in the middle part of Fig. 1 and consists of a Triangular Rollable And Collapsible (TRAC) boom [33] wrapped around a 30 cm diameter drum. The TRAC boom is chosen for flexibility during deployment and stiffness during retraction, necessary to maintain control of the SARP throughout sampling. This reduces risk compared to any rigid coupling to the surface and prevents the SARP from impacting the spacecraft at any time. The SARP is the SAS projectile portion that collects the nucleus sample. The SARP outer sheath serves as the surface impactor and does not return to the spacecraft. Inside the outer sheath are mounted the inner sheath, cartridge, and mechanisms necessary to complete sampling. Each sample cartridge has a 298 cm³ sample bay and a spring-loaded knife-edge door at its opening that closes to encapsulate the captured sample. Both systems, BRAD and SARP are developed and tested at NASA GSFC. The SAS launcher is a DLR contribution to the proposed CORSAIR mission.

4. Sample acquisition and handling

An Altimetric Laser with heritage from the OSIRIS-REx mission measures the range between the spacecraft and comet surface with at least ± 1 m range resolution [34]. The sampling event starts with a spacecraft command to the SAS at about 10 m above the comet surface. The command triggers the launcher accelerating the SARP to penetrate ≥ 10 cm into the surface. Because of the flexibility of the TRAC boom and the emergency brake of the BRAD, the SAS design inherently accepts a wider range of spacecraft to surface distances than the range given by the accuracy of the Altimetric Laser. Upon surface impact, the SARP outer sheath bears the impact forces and breaks up comet material for ingestion. In case of shorter than nominal distances and depending on the density and compressive strength of the material, the SARP might penetrate deeper into the surface than the 10 cm depth requirement. In terms of science return, this is a strength of the proposed sampling technology compared to other methods with predefined sampling depths. An artist impression of the sampling event with deployed TRAC boom and SARP is shown in Fig. 2. The SARP comes to

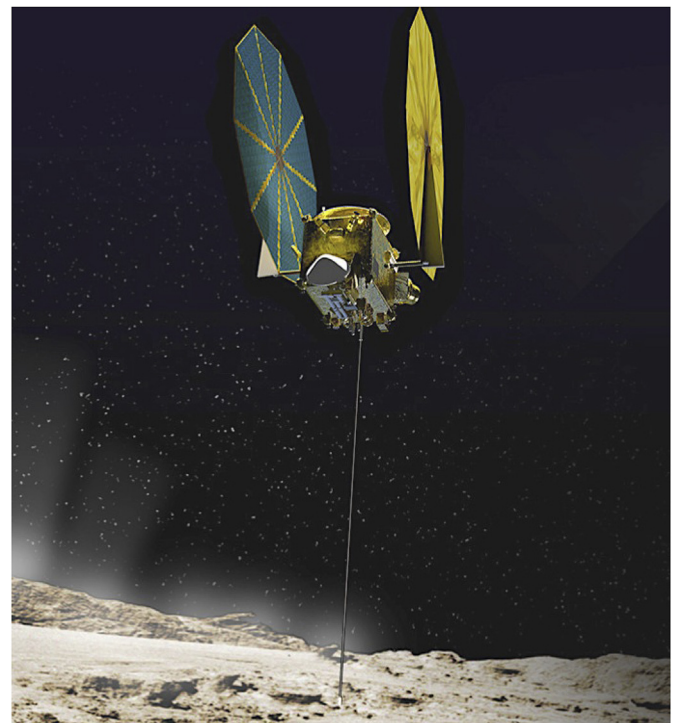


Fig. 2. Artist impression of CORSAIR sampling event.

rest through comet resistance, retraction system braking, or both. A timer closes the cartridge door, cutting through the cometary material and fully encapsulating the sample. Subsequently, the inner part of the SARP separates from the outer sheath and the BRAD is activated for SARP retraction. An Automatic Dynamic Analysis of Mechanical Systems (ADAMS) of the entire sampling event has been completed to validate TRAC boom properties, in particular the critical buckling moment, to exclude the possibility of contact of the boom with the spacecraft during launch and retraction.

The SARP was designed such that in case of harder comet material, the risk of getting stuck is mitigated. The inner part of the SARP decouples from the outer sheath after sample acquisition and the outer sheath is left behind allowing the cartridge to be retrieved without getting stuck. Moreover, a guillotine was foreseen as additional safety measure (see Fig. 1). If the spacecraft would have detected a certain threshold of motion towards the comet upon SARP retraction, this mechanism would have cut the TRAC boom of the used SAS unit. In the course of this study, also the extraction via a pulling force profile with short repetitive strokes was investigated but not implemented in the current design. In the case of very loose underground, the outer sheath possibly does not stick to the cometary material. For this scenario, a spring loaded release mechanism would have ensured a decoupling from the outer sheath prior to retraction.

After the sample has been acquired, the spacecraft departs the comet and at a safe distance, imaging of the SARP is used to provide an initial assessment. These images are analyzed on the ground and, once reviewed, a robotic arm extracts the cartridge and transfers it to a Sample Handling Station (SHS) for devolatilization and later from the SHS to the Sample Storage System (SSS) [35]. The robotic arm is a DLR contribution to the proposed mission. It grasps, removes, transfers, inserts and releases the cartridge fully autonomously through the use of force feedback and torque control without visual targeting [36–38].

5. Launcher design

The launcher is part of the SAS and transfers the required momentum to the SARP and BRAD. A sufficiently high SARP velocity must be chosen, in order to penetrate the comet surface deep enough for material with the

hardest expected compressive strength. Obtaining primitive cometary material requires the collection of samples to a depth of at least 10 cm [6,7]. The majority of estimates of the compressive strengths of cometary surface materials are less than tens of kilopascals [39–43]. However, Rosetta showed that the sublimation and redeposition cycles near the surface can cause sintering of icy material [44], resulting in compressive strengths of ~ 1 MPa or more [45,46]. The first touchdown of the Rosetta lander Philae on the surface of comet 67P/Churyumov-Gerasimenko revealed a granular soft surface with a compressive strength of ~ 1 kPa at least 20 cm thick, possibly on top of a more rigid layer [26]. Higher-strength material is present in some regions [44], but this material is not representative of the bulk nucleus [41].

Thus, a sampling system that penetrates a range of material strengths, including material >1 MPa, is required to maximize the likelihood of acquiring the most primitive and unaltered cometary material that resides below the processed surface layers. From an engineering standpoint, a maximum expected compressive strength of 2 MPa is assumed. Further important material parameters are density and porosity. For comet 67P/Churyumov-Gerasimenko, porosity in a range between 70% and 85% [47–49] has been measured. Comet porosity on the surface can be lower than these global values. Spohn et al. mention surface porosities of 30–65% [44].

NASA GSFC performed SARP penetration tests into porous glass foam of different compressive strengths with a cold gas launching system. The compressive strengths ranging from 800 kPa to 2.4 MPa were determined in a uniaxial test configuration [50,51]. Due to its consolidated, not granular and brittle nature, glass foam may be not fully representative as comet analog in any respect [52]. However, the material is long-term stable and readily available. Therefore, it offers advantages in terms of test reproducibility. Furthermore, glass foam is available in a broad range of compressive strengths which is a relevant parameter for the penetration characteristics [53]. Finally, it is highly

porous similar to granular material. The porosities of the used glass foam are higher than 90% exceeding the calculated values for comet 67P/Churyumov-Gerasimenko. A test with an impact velocity of 33.4 m/s and with an analog material of 2.4 MPa compressive strength revealed a penetration depth of 14.6 cm. In case of the pyro-driven launcher developed at DLR, the design velocity is in the range between 35 m/s and 50 m/s. Therefore, enough margin is provided for material with higher compressive strength.

Further important constraints and requirements are the minimization of impulse and force exerted on the spacecraft, the reduction of system mass and the contamination control of the retrieved samples. Mainly because of high-energy densities, it was decided early in the study phase to use a pyrotechnical system. Prior to that, alternatives such as electromagnetic, cold gas and spring systems have been studied as well. However, these concepts require considerable more allocated mass and – in case of an electromagnetic design – would not be compatible with existing constraints concerning the spacecraft avionics. The safe operation of a pyrotechnical system on a spacecraft can be ensured by integrating adequate safety measures, such as an electronic safe, arm and fire device.

5.1. Design evolution

Launcher development began at DLR in 2013. The initial SAS concept had a dual tether retraction system consisting of two metallic tapes laterally attached to the launcher structure. The tapes are rolled up in stowed position and deploy during sampling with the ends attached to the SARP. Because of this lateral configuration, a smaller diameter launcher with a single piston rod was designed. The upper sketch in Fig. 3 shows the building blocks of this initial launcher concept.

In contrast to the Rosetta/Philae harpoons [25], the propellant is ignited via an initiator instead of a bridge wire. The cause of the Philae harpoon malfunction could not unambiguously identified [54]. However, the bridge

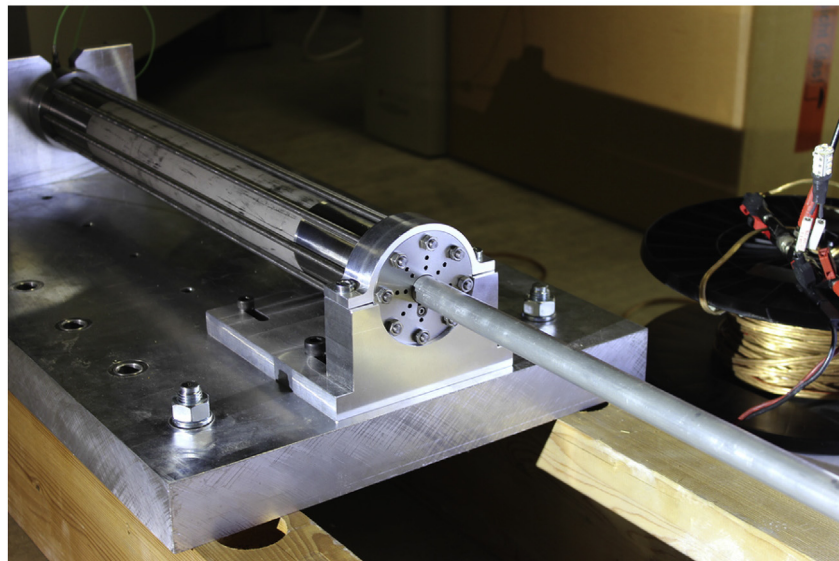
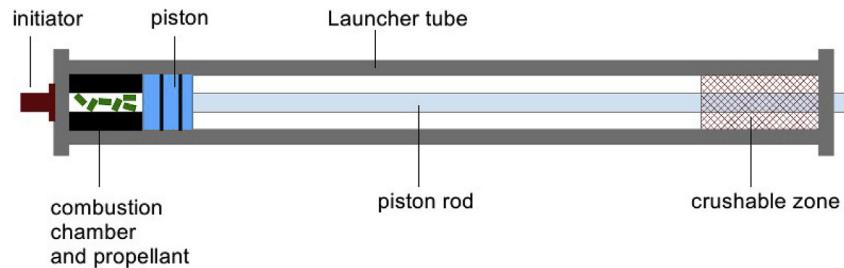


Fig. 3. Top: Initial launcher concept. Bottom: Launcher version 1.0 with deployed piston rod. Not shown here is the dummy mass which is a steel body of $m_{DM} = 2.987$ kg emulating the inertia of SARP ($m_{SARP} = 2$ kg) and retraction system ($m_{eff} = 0.987$ kg).

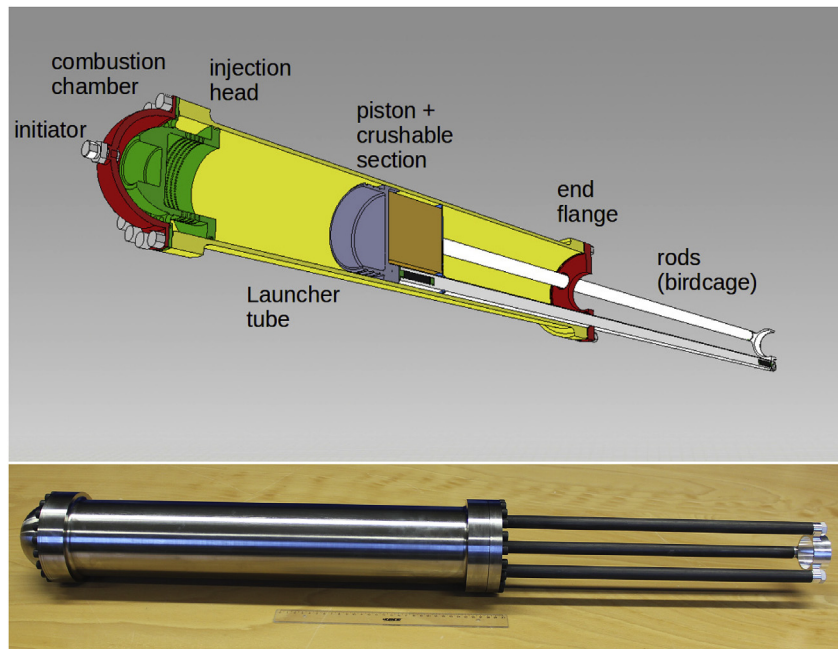


Fig. 4. Top: Sectional view of launcher baseline design. Piston seals are not shown here. Bottom: Launcher version 2.0 hardware.

wire technique seems to be less adequate in space environments because it relies on a sufficient large thermal contact between bridge wire and propellant grains which is partly provided by gas molecules trapped inside the combustion chamber. Initiators make also use of a bridge wire for thermal activation. However, the activation energy is not directly transferred to propellant grains. Initiators contain highly stable pyrotechnic substances with fast reaction rates. Intimate contact between bridge wire and explosive is assured through a slurry preparation process. Thus, thermal activation of the initiator and subsequently of the propellant is ensured even if residual gas is absent in the combustion chamber. For the CORSAIR launcher, the commercial initiator PyroGlobe GG821 is used. In a later stage, this can be replaced by a space-qualified counterpart, e.g. the NASA Standard Initiator (NSI), or alternatively, space-qualification of a commercially available initiator is provided.

Main ingredients of the propellant mixture are 7-perforation Nitrocellulose grains which are placed inside a dedicated combustion chamber (see upper sketch in Fig. 3). The combustion chamber is a cylindrically shaped inlay and is manufactured from polyoxymethylene (POM). The combustion gas generates pressure pushing the piston with the attached piston rod. The prototype should prove the feasibility of the concept and no space-qualified items have been used. For sealing, rubber O-rings are used. At the end of the launcher tube, a crushable zone absorbs the kinetic energy of piston and rod. Here, a stack of several Aluminum honeycomb rings is used.

For the first prototype – version 1.0 – the piston rod was manufactured from an Aluminum tube. However, with increasing propellant charge, this turned out not to withstand critical buckling loads. Therefore, version 1.5 was built with a piston rod made from high-modulus carbon composite material. The outstanding stiffness-to-mass-ratio proved to sustain higher loads. Furthermore, the crushable was replaced by an Aluminum honeycomb structure with higher density yielding higher crush strengths and shorter stopping distances.

5.2. Baseline design

Later, the retraction system design was changed to a single boom concept, providing better performance on both boom deployment and retraction. This had major implications on the launcher design. To accommodate the centrally guided composite boom, first, a launcher tube

diameter twice as large as in the previous version had to be chosen, and second, the rod configuration had to be changed. Due to the increased inner tube diameter of 100 mm, a much higher gas production was needed. Therefore, it was decided to implement a high-low pressure system with two separate chambers [55,56].

In case of the baseline design shown in Fig. 4, the propellant burns in a combustion chamber, and the produced gas passes an injection head – a flow-restricting device – before entering the launcher tube. Because of the higher and steady gas pressure in the combustion chamber, propellant burning is optimized, whereas the pressure profile inside the launcher tube is more uniform, attenuating the acceleration peak. Ultimately, the high-low pressure approach reduces the mass of the launcher subsystem and solves packing of the propellant which is stored in a dedicated powder chamber. Pyrotechnic high-low pressure systems have been successfully operated in various NASA space missions, in particular for parachute mortar systems [57,58].

Although the baseline design – version 2.0 – uses a different chamber design compared to former versions, some parts have been adopted from version 1.5, notably the high-modulus carbon composite rods and the higher strength crushable material. Launcher version 2.0 is composed of mass optimized and primarily of space-proof parts. Most parts are manufactured from Titanium grade 5. Thin walls down to 2 mm have been manufactured for the launcher tube. The piston includes three spring-energized and reinforced polytetrafluoroethylene (PTFE) seals. The momentum is transferred from the piston to the SARP via three piston rods arranged circularly around the centrally/axially guided boom. The boom is deployed from a sidewise mounted reel (see Fig. 1). For the boom feed-in, enough clearance in both the lateral and axial direction has to be provided in this rod configuration, which is also referred to as *birdcage*.

In order to provide enough axial offset, longer rods than for the first generation launcher are required. Since longer rods increase buckling loads, the material selection and dimensioning of the rods have been carried out with special care. Fig. 5 shows the numerical and analytical studies performed on this topic. The upper image is an example of a Finite Element Method (FEM) simulation with a lateral force applied to one end of the birdcage. Lateral forces are mostly relevant for the terrestrial test setup with horizontal launcher orientation and 1 g environment.

The lower plot in Fig. 5 shows the results of an analytical calculation using the Euler-buckling formula modified to composite materials

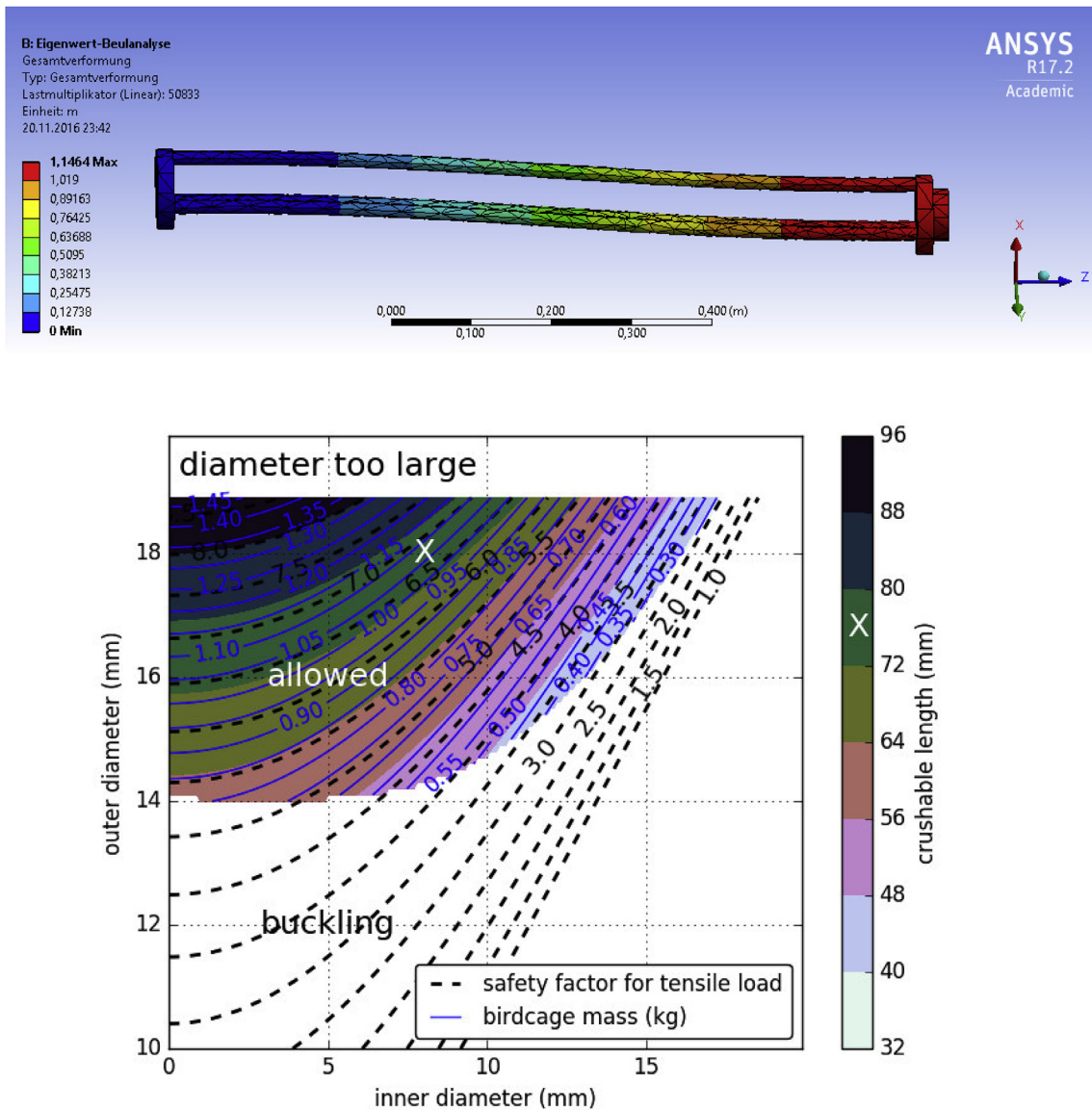


Fig. 5. Top: FEM simulation of mechanical loads on birdcage assembly. Bottom: Dimensioning of carbon composite birdcage rods.

[59,60]. The colored region denotes the allowed rod configurations as a function of inner and outer rod diameter, i.e. those dimensions fitting to the geometrical constraints of the BRAD system and withstanding buckling. Since the birdcage mass depends on the rod dimensions, the resulting kinetic energy and required length of the crushable are also functions of the rod dimensions. This is reflected by the color code. In addition, the birdcage mass and the safety-factor for tensile load during deceleration are plotted on the same graph. The white X sign marks the chosen rod configuration for the launcher hardware.

6. Launcher testing

All launcher versions have been tested in stand-alone experiments, i.e., using dummy masses instead of the SARP and the retraction system. By doing this, SARP and launcher testing can be performed independently from each other. The rationale behind this approach is that the inertias of SARP and BRAD can be combined to an effective mass reflecting the mass of the SARP ($m_{SARP} = 2 \text{ kg}$ for all versions) plus an extra mass, which is equivalent to the rotational inertia of the retraction system. Fig. 6 shows the test setup with the horizontally mounted launcher. After completing the piston stroke, the dummy mass

is released. Then, the dummy mass is in free flight before it is absorbed in a box filled with padding material (not shown).

A set of experimental data is acquired at each test: A high-speed camera with frame rates up to 20000 fps records the motion of piston and dummy mass. Videos of tests performed with launcher versions 1.5 and 2.0 can be found in Ref. [61]. With the help of post-processing tracking, fitting and derivation algorithms, the velocity and acceleration profiles are deduced from the positional data. A piezoelectric pressure sensor monitors the pressure profile inside the combustion chamber. Pressure sensor and initiator are mounted on a T-piece converging to the combustion chamber. Optionally, the pyro-shock can be measured. This is basically a vibration spectrum of the launcher structure.

7. Launcher theory – internal ballistics

Traditionally, the design of pyrotechnic devices is a process driven to a large extent by trial and error. Experiments tend to be expensive, time-consuming and have high risk potential. Furthermore, some quantities such as time and space-resolved gas temperature are practically inaccessible or require complex and costly nonstandard instrumentation. In order to minimize these disadvantages and streamline

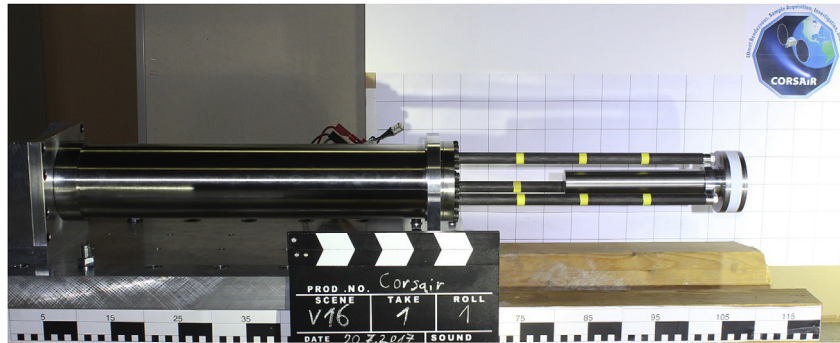


Fig. 6. Testing of launcher version 2.0 with three circularly arranged piston rods (*birdcage* configuration). The elongated metallic body attached to the *birdcage* is the dummy mass. A higher dummy mass of $m_{DM} = 4.65$ kg is used taking into account the increased moment of inertia of the BRAD ($m_{off} = 2.65$ kg) compared to the inertias of the lateral drums of the first generation SAS.

the development process, numerical modeling of the internal ballistics became a main effort of this work. In the beginning, stand-alone program codes have been written for solving individual and elementary problems. When the project and the knowledge of underlying processes further developed, these efforts converged into a more complete and complex simulation framework. The overall goal of the modeling efforts is to reflect the entire reaction chain beginning with the burning of propellant grains to gas-dynamic processes and finally the piston and SARP motion. Main objectives are supporting the launcher development process and predicting the launcher behavior for future tests.

For the implementation of the model, either the Modelica [62,63] or the Assimulo [64] frameworks have been used. Modelica is a declarative and object-oriented framework and supports *acausal* modeling, i.e., solves implicit systems of equations. The acausality makes Modelica library classes more reusable than traditional classes containing assignment statements where the input-output causality is fixed. Moreover, the open-source version OpenModelica includes graphical tools for both programming and data visualization. There are detailed libraries available for many domains such as electric circuits, mechanics, thermodynamics and fluids. Just as Modelica, the framework Assimulo supports discontinuous systems. There are present various discontinuities in the internal ballistics problem such as discrete changes of propellant burning, burst opening of individual injector holes, change from choked flow to subsonic conditions and transition from piston acceleration to deceleration at the end of piston stroke. Usually, the appearance of discontinuities is not triggered explicitly by time but depends on variables which are computed solutions of the ordinary differential equation (ODE) system.

Starting with propellant burning and terminating with the computed piston motion, the most relevant physical processes of the entire reaction chain have been implemented in the internal ballistic models. Solid propellant changes its geometric shape as the surface successively turns to gas (see Fig. 7). Thus, the total rate at which combustion gas is produced can be controlled by the geometric shape of the propellant grains. In general, the geometry is designed to achieve a progressive, degressive or neutral flow rate. Propellants come in complex geometric shapes and a mixture of different geometries with 7-perforation Nitrocellulose grains as main ingredient is used in the launcher. In order to reflect the change in geometry mathematically, an effective shape function $\phi(z)$ is used with z being a dimensionless value between zero and one representing the percentage of burnt charge mass. A shape function curve for 7-perforation propellant can be found for example in section 2.1.5.3 of reference [56]. This curve can be fitted in steps by two polynomial functions for the two branches representing bulk and slivers burning. Thus, the problem of geometric shape change is reduced to two piecewise defined functions with constant coefficients. Furthermore, the combustion rate depends on the chamber pressure. In internal ballistics [56,65,66], the regression rate usually follows the empirical formula as expressed in this correlation:

$$\dot{r} = \beta p^\alpha \quad (1)$$

with \dot{r} being the regression rate of the propellant, β the linear burn rate and α an exponent to the pressure p . Depending on the chamber pressure range, β and α can be assumed to be constant or a piecewise definition of these parameters is implemented for different pressure regimes. Measurements of the linear burning rates against chamber pressure and adequate fits reveal these parameters. Plots of measured linear burning rates for comparable nitrocellulose propellants can be found for example in Ref. [67]. For the launcher models, the propellant parameters β and α have been found through iterative adaption and comparison with test results of launcher versions 1.0 and 1.5 which are equivalent in terms of internal ballistics. The set of propellant parameters showing maximum consistency with all test results of the first launcher versions has been kept constant from henceforward and subsequently used for the internal ballistic model of launcher version 2.0 (baseline design). Since the propellant composition was unchanged within the test series, propellant properties can be regarded as constant which justifies the explained approach. However, it should be noted here that best simulation results could be achieved by an independent measurement of the propellant burning rate. Usually, the pressure dependent regression stated in equation (1) is predominant over

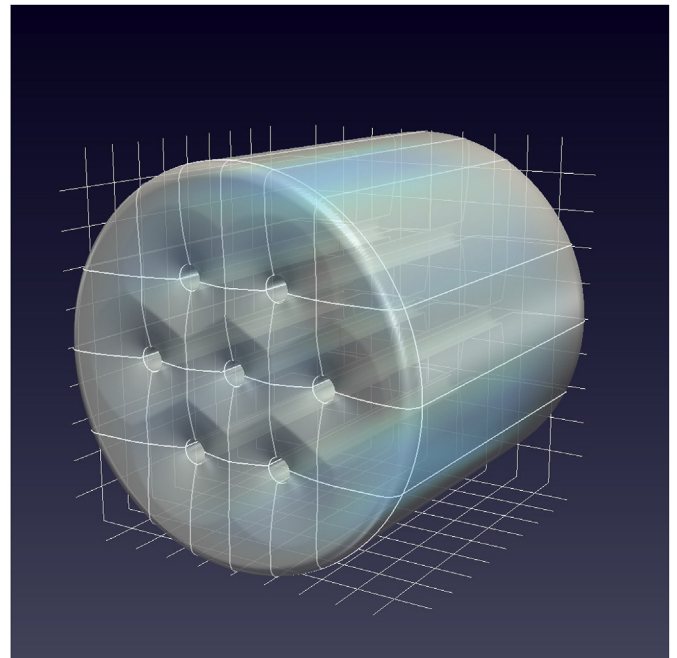


Fig. 7. Simulated burning of a 7-perforation propellant grain. The simulation results help to find the effective shape function of the propellant.

geometric shape changes with respect to the system response. The internal ballistic models of the launcher show that a variance of the shape function has only little effect on the pressure and motion profiles. Thus, the shape function can be simplified to $\phi(z) = 1$ as a good approximation.

The combustion gas mixture is modeled using fixed and averaged properties for the adiabatic constant κ and the molar mass M . Given the mole fractions of the molecular species, the equilibrium gas properties are either deduced from look-up tables or calculated by the NASA program code *Chemical Equilibrium with Applications* (CEA) [68]. In internal ballistics (see for example reference [66]), often the Noble-Abel equation is used for describing the gas behavior. In this context, a covolume takes into account the interaction of gas molecules at high pressures. However, the built launcher versions use relative large volumes entailing lower gas pressures than typically present in pyrotechnic systems. Thus, the ideal gas law describes the gas behavior with sufficient accuracy:

$$pV = \frac{m}{M}RT \quad (2)$$

where V is the chamber volume, m the gas mass, T the gas temperature and R the universal gas constant. The expanding gas results in a piston movement and Newton's law of motion correlates the force originating from the gas pressures with the acceleration of the piston:

$$m_S \ddot{x} = pA \quad (3)$$

with m_S being the total accelerated mass, x the piston displacement, \dot{x} and \ddot{x} its derivatives with respect to time and A the inner cross sectional area of the launcher.

In case of the baseline design, there is a flow restricting device which limits the mass flow rate. In the upper image of Fig. 4, this device is referred to as injection head. The rate of gas generated by propellant burning is in balance with the mass rates flowing in and out the combustion chamber and launcher tube:

$$\dot{m}_{CC} + \dot{m}_{LT} = \beta p_{CC}^{\alpha} \quad (4)$$

with m_{CC} and m_{LT} being the gas masses in combustion chamber and launcher tube, and p_{CC} the combustion chamber pressure. A maximum number of 400 pinholes restrict the gas flow from the combustion chamber to the launcher tube. The pinholes are modeled as an ideal adiabatic nozzle where a discharge coefficient C_D takes into account the shape of the holes [69]. Depending on the pressure ratios, two different formulas apply for the gas flow rate from combustion chamber to launcher tube. For choked flow conditions with $\frac{p_{CC}}{p_{LT}} \geq r_{cri}$, the mass flow rate is:

$$\dot{m}_{LT} = C_D A_h \sqrt{\kappa \frac{p_{CC} m_{CC}}{V_{CC}} \left(\frac{2}{\kappa + 1} \right)^{\frac{\kappa+1}{\kappa}}} \quad (5)$$

Whereas, for sub-sonic flow conditions with $\frac{p_{CC}}{p_{LT}} < r_{cri}$, the mass flow rate becomes:

$$\dot{m}_{LT} = C_D A_h \sqrt{\frac{2\kappa}{\kappa - 1} \frac{p_{CC} m_{CC}}{V_{CC}} \left[\left(\frac{p_{LT}}{p_{CC}} \right)^{\frac{2}{\kappa}} - \left(\frac{p_{LT}}{p_{CC}} \right)^{\frac{\kappa+1}{\kappa}} \right]} \quad (6)$$

with V_{CC} being the combustion chamber volume, p_{LT} the launcher tube pressure and A_h the total cross sectional area of all opened pinholes. The critical pressure ratio is defined as:

$$r_{cri} = \left(\frac{\kappa + 1}{2} \right)^{\frac{\kappa}{\kappa - 1}} \quad (7)$$

The injector pinholes are covered by a thin Aluminum membrane bursting on the individual holes if a certain pressure difference between both chambers is exceeded. The membrane has been placed on the injector head for two reasons. First, this mechanism prevents premature pressure compensation which would compromise propellant burning.

Second, the membrane limits the amount of open pinholes favoring choked flow conditions. Due to minor differences in spatial pressure distribution and membrane properties, the burst pressure differs slightly from one pinhole to another. Therefore, bursting does not occur at the same time for all pinholes. In the model, this effect is taken into account by assuming a Gaussian distribution with a mean value μ_p and a standard deviation σ_p for the burst pressure. In case of the two-chamber baseline design, there is an unsteady-state flow [70] between both chambers which is described by two energy equations for each separate control volume:

$$d(mu)_{\text{control volume}} + \Delta(hdm)_{\text{flowing streams}} = \sum \delta Q - \sum \delta W \quad (8)$$

with u being the specific internal energy, h the specific enthalpy, $\sum \delta Q$ the sum of all heat and $\sum \delta W$ the sum of all work transferred into and out the corresponding control volume. The work term becomes non-zero for the launcher tube. It is assumed that there are no energy losses, for example through heat transfer or piston friction. Adiabatic conditions are primarily justified since the piston stroke is fast (~ 20 ms) compared to heat exchange with the environment. Thus, the heat term becomes zero for both chambers. The thermodynamic potentials u and h are functions of the variables p , x , m and T . Finally, the ODEs stated above are written as a system of six first-order ODEs and solved numerically by an adequate integrator for the two-chamber baseline design.

8. Results

Table 1 summarizes key parameters and results of a consistent set of tests. Other tests with changed propellant mixture or non-nominal piston rod behavior are not listed here with the exception of test V9. In test V9, the highest dummy mass velocity was reached and a failure of the piston rod was observed. Since this failure occurred due to excessive tensile loads on the rod during piston stopping – i.e. after the acceleration phase – the results of V9 are still regarded as consistent within the presented data set. It should be noted, that the work presented here focused on demonstrating feasibility of the concept. An optimal set of launcher parameters was not known from the beginning and both approaches, testing and numerical modeling reciprocally stimulated each other. The launcher test series performed during this development phase rather covers most of the parameter space than provides a statistically sufficient number of tests for one particular configuration.

For each launcher version, propellant charge m_p was increased step by step. Furthermore, the combustion chamber volume V_{CC} of the first generation launcher can be adjusted by drilling the POM inlet (see upper sketch in Fig. 3). By comparing tests V9 and V10, the relevance of the parameter V_{CC} becomes clear. Test V9 used more propellant but had the same combustion chamber volume resulting in higher peak pressure and peak acceleration than in test V10. The importance of parameter V_{CC} can also be confirmed by comparing tests V1 and V9. Both tests showed comparable values for peak pressure p_{max} and peak acceleration a_{max} . However, test V9 used a charge m_p 3.67 times higher and had a volume V_{CC} 5.47 times larger than in test V1. This means that V_{CC} is a relevant design parameter for adjusting the resulting peak acceleration.

For test V10, a high-modulus carbon composite rod was used instead of the metallic rod in launcher version 1.0. The piston assembly had the same mass as in the metallic version. Therefore, both versions can be regarded as equivalent in terms of internal ballistics. Due to the increased stiffness of the carbon composite material, the rod withstands higher peak accelerations and due to the increased tensile strength of the assembly, a crushable material with enhanced crush strength could be used resulting in shorter stopping distances and a longer free acceleration length l_f .

As can be seen from Table 1, the pressure values in the two last tests using launcher version 2.0 are much lower than in those tests using the one-chamber design. The first values of p_{max} correspond to the measured combustion chamber pressures; the value in V11 is missing due to

Table 1

Selected launcher tests. First two columns denote test number and launcher version. Dummy mass was 2.987 kg for launcher versions 1.0–1.5, and 4.65 kg for launcher version 2.0. m_p : propellant charge, V_{CC} : combustion chamber volume, l_f : free acceleration length, p_{max} : peak pressure (two values for launcher version 2.0 corresponding to combustion chamber and launcher tube), a_{max} : peak piston acceleration in multiples of gravity (g), v_{DM} : final dummy mass velocity.

Test	ver.	m_p (g)	V_{CC} (cm ³)	l_f (mm)	p_{max} (MPa)	a_{max} (g)	v_{DM} (m/s)
V1	1.0	3.0	8.1	376	15.5	771	35
V3	1.0	6.5	22.6	376	11.0	573	45
V9	1.0	11.0	44.3	376	15.0	777	62
V10	1.5	8.3	44.3	448	11.0	540	51
V11	2.0	5.7	222.0	406	-/1.1	142	20
V16	2.0	15.0	222.0	406	5.3/2.8	348	31.4

instrumentation reasons. The lower pressure as compared to the one-chamber design is the consequence of a larger combustion chamber volume amongst others. The second values correspond to the peak pressures in the launcher tube. These values have been reconstructed from the acceleration profile assuming a uniform pressure distribution within the launcher tube. So far, the final dummy mass velocities have been lower than in tests V1 – V10. However, a much higher dummy mass of 4.65 kg has been used instead of the 2.987 kg mass taking into account the increased inertia of the modified retraction system. Furthermore, the mass of the piston assembly increased as well, and a higher gas production is needed in order to pressurize the larger volume.

Fig. 8 shows the motion profile of tests V3, V10, V11 and V16. Solid lines correspond to experimental data and dashed lines to numerically modeled data. The solid curves in the upper plots show the piston position which has been directly measured through the described tracking method. Both, experimental velocity (middle plots) and acceleration (lower plots) have been derived via differentiating the fitted positional data. From all tests performed with a one-chamber launcher, V10 uses the most optimized configuration of parameters m_p and V_{CC} . The final dummy mass velocity was at the upper end of the design range, while the peak acceleration was comparably low. Experimental and numerically modeled data coincide well in case of the one-chamber design. For the baseline design, there are larger discrepancies between simulated and measured motion profiles which can partly be explained by the approximations made for the internal ballistics model. For instance, the parameters determining propellant burning are set constant. For greater accuracy, these parameters could be adapted for different pressure regimes as described above.

9. Conclusions and outlook

In summary, an overview of the proposed CORSAIR mission and the harpoon-based comet sampling method has been given. After describing the building blocks of the Sample Acquisition System, this paper highlights the pyro-driven launcher, which provides the required kinetic energy to the Sample Acquisition and Retrieval Projectile. Launcher design requirements are mainly derived from scientific requirements (sampling depth) and the maximum expected compressive strength of the comet surface. Subsequently, the design evolution of

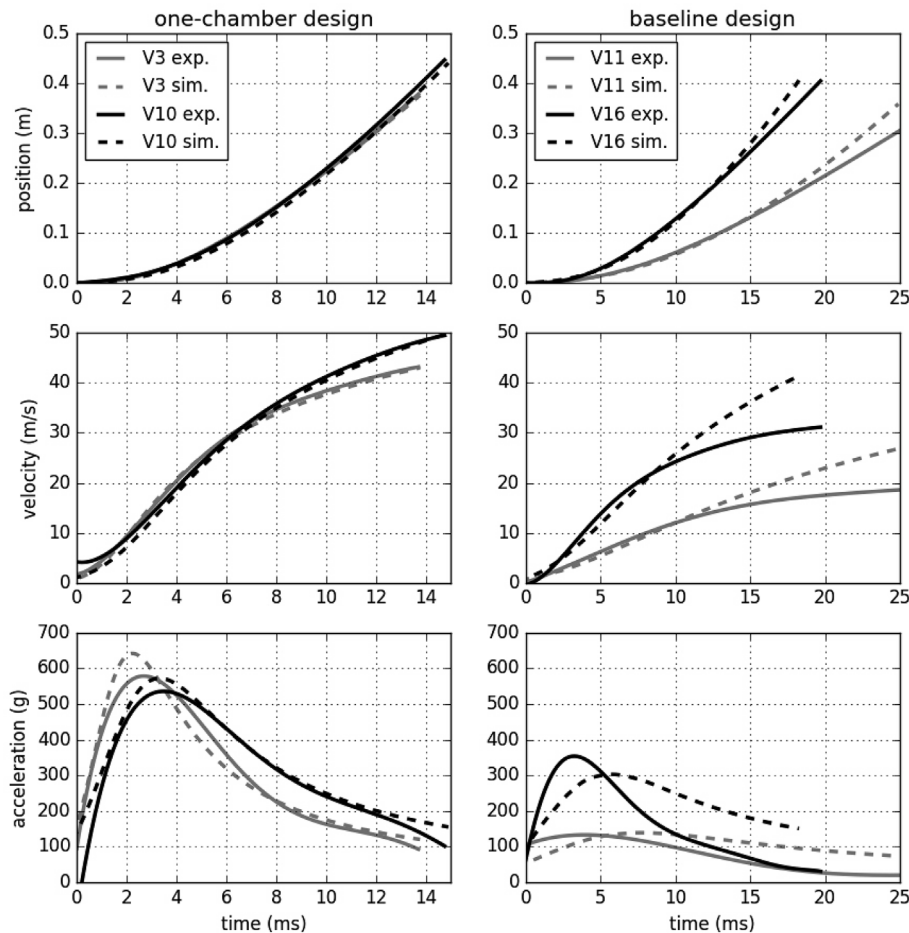


Fig. 8. Left: Piston motion profiles of tests V3 and V10 (one-chamber design, launcher versions 1.0/1.5). Right: Piston motion profiles of tests V11 and V16 (baseline design, launcher version 2.0). Comparison of experimental (solid lines) with simulated data (dashed lines).

different launcher versions is presented, terminating in the current baseline design that is compatible with a novel retraction system using a single composite boom structure. Afterwards, the setup for launcher stand-alone tests is described and the modeling framework for the internal ballistics of the launcher is outlined. Finally, the test results are discussed and compared with simulation data. Both, test and simulation results support the feasibility of the launcher concept for comet sample acquisition.

The final dummy mass velocity of the last presented test (Table 1) with the baseline design is close to the lower end of the defined design range. Because of the complex and highly dynamic interaction between design parameters and piston motion, a further increase of propellant charge without having modified other design parameters might have only little effect on the final velocity. The described modeling framework supports the development process. An extension of this framework for systematic scans and evaluation of the entire parameter space would probably find a set of optimized design parameters for the baseline design. After having implemented these parameters into the hardware, launcher performance should be verified and a statistically sufficient number of tests under same conditions should be executed.

References

- J.M. Greenberg, What are comets made of? A model based on interstellar dust, *Comets* 131 (1982) 163.
- F.L. Whipple, The cometary nucleus: current concepts, *Exploration of Halley's Comet*, Springer, 1988, pp. 852–858.
- P. Ehrenfreund, S.B. Charnley, D.H. Wooden, From interstellar material to cometary particles and molecules, *Comets II* (2004) 115–133.
- F.J. Ciesla, S.B. Charnley, The Physics and Chemistry of Nebular Evolution, Meteorites and the Early Solar System II, vol. 943, (2006), pp. 209–230.
- S.A. Sandford, N.L. Chabot, N. Delo Russo, J.C. Leary, E.L. Reynolds, H.A. Weaver, D.H. Wooden, The CORSAIR Team, CORSAIR (COMet Rendezvous, Sample Acquisition, Investigation, and Return): A New Frontiers Mission Concept to Collect Samples from a Comet and Return them to Earth for Study, 80th Annual Meeting of the Meteoritical Society, 2017 LPI Contrib. No. 1987.
- G.H. Fountain, et al., Comet Surface Sample Study Report, Tech. Rep. SDO-11998, NASA, Prepared for NASA's Planetary Science Division, 30 April 2008, Washington, DC, 2008.
- J. Veverka, L. Johnson, E. Reynolds, Comet Surface Sample Return (CSSR) Mission - NASA Planetary Science Decadal Survey Mission Concept Study, Tech. rep., NASA (2011), http://sites.nationalacademies.org/SSB/SSB_059331.
- D.S. Burnett, B.L. Barraclough, R. Bennett, M. Neugebauer, L.P. Oldham, C.N. Sasaki, D. Sevilla, N. Smith, E. Stansbery, D. Sweetnam, et al., The Genesis discovery mission: return of solar matter to Earth, *Space Sci. Rev.* 105 (3–4) (2003) 509–534.
- D.E. Brownlee, P. Tsou, J.D. Anderson, M.S. Hanner, R.L. Newburn, Z. Sekanina, B. C. Clark, F. Hörz, M.E. Zolensky, J. Kissel, et al., Stardust: Comet and interstellar dust sample return mission, *J. Geophys. Res.* 108 (E10).
- D. Brownlee, The Stardust mission: analyzing samples from the edge of the solar system, *Annu. Rev. Earth Planet. Sci.* 42 (2014) 179–205.
- H. Sawada, R. Okazaki, S. Tachibana, K. Sakamoto, Y. Takano, C. Okamoto, H. Yano, Y. Miura, M. Abe, S. Hasegawa, et al., Hayabusa2 Sampler: Collection of Asteroidal Surface Material, *Space Sci. Rev.* 208 (1–4) (2017) 81–106.
- O.S. Barnouin-Jha, K. Barnouin-Jha, A.F. Cheng, C. Willey, A. Sadilek, Sampling a Planetary Surface with a Pyrotechnic Rock Chipper, *Aerospace Conference*, 2004. Proceedings. 2004 IEEE, vol. 1, IEEE, 2004.
- B.C. Clark, E.B. Bierhaus, J.W. Harris, K.S. Payne, D.W. Wurts, R.D. Dubisher, S.L. Deden, TAGSAM: a Gas-driven System for Collecting Samples from Solar System Bodies, *Aerospace Conference*, 2016 IEEE, IEEE, 2016, pp. 1–8.
- D.S. Lauretta, S.S. Balram-Knutson, E. Beshore, W.V. Boynton, C.D. d'Aubigny, D.N. DellaGiustina, H.L. Enos, D.R. Golish, C.W. Hergenrother, E.S. Howell, et al., OSIRIS-REx: sample return from asteroid (101955) Bennu, *Space Sci. Rev.* 212 (1–2) (2017) 925–984.
- R. Bonitz, The Brush Wheel Sampler – a Sampling Device for Small-body Touch-and-Go Missions, *Aerospace Conference*, 2012 IEEE, IEEE, 2012, pp. 1–6.
- P. Backes, S. Moreland, H. Manohara, J. Green, J. Grimes-York, M. Badescu, P. Vieira, R. Toda, E. Carey, G. Peters, Experimental results with the blade sampling chain for comet surface sampling, *Aerospace Conference*, 2016 IEEE, IEEE, 2016, pp. 1–10.
- P. Backes, S. Moreland, F. Rehnmark, M. Badescu, K. Zacny, R. Wei, G. Adams, R. Toda, P. Vieira, E. Carey, et al., BiBlade sampling tool validation for comet surface environments, *Aerospace Conference*, 2017 IEEE, IEEE, 2017, pp. 1–20.
- Y. Bar-Cohen, K. Zacny, *Drilling in Extreme Environments: Penetration and Sampling on Earth and Other Planets*, John Wiley & Sons, 2009.
- K. Zacny, Y. Bar-Cohen, M. Brennan, G. Briggs, G. Cooper, K. Davis, B. Dolgin, D. Glaser, B. Glass, S. Gorevan, et al., Drilling systems for extraterrestrial subsurface exploration, *Astrobiology* 8 (3) (2008) 665–706.
- N.L. Johnson, *Handbook of Soviet Lunar and Planetary Exploration* vol. 80, NASA STI/Recon Technical Report A, 1979.
- S.P. Gorevan, T. Myrick, K. Davis, J.J. Chau, P. Bartlett, S. Mukherjee, R. Anderson, S.W. Squyres, R.E. Arvidson, M.B. Madsen, et al., Rock abrasion tool: Mars exploration rover mission, *J. Geophys. Res. Plan* 108 (E12) (2003).
- R.G. Bonitz, L. Shiraishi, M. Robinson, R.E. Arvidson, P.C. Chu, J.J. Wilson, K.R. Davis, G. Paulsen, A.G. Kusak, D. Archer, et al., NASA Mars 2007 Phoenix lander robotic arm and icy soil acquisition device, *J. Geophys. Res. Plan* 113 (E3) (2008).
- R.C. Anderson, L. Jandura, A.B. Okon, D. Sunshine, C. Roumeliotis, L.W. Beegle, J. Hurowitz, B. Kennedy, D. Limonadi, S. McCloskey, et al., Collecting samples in Gale Crater, Mars; an overview of the Mars Science Laboratory sample acquisition, sample processing and handling system, *Space Sci. Rev.* 170 (1–4) (2012) 57–75.
- A.E. Finzi, F.B. Zazzera, C. Dainese, F. Malnati, P.G. Magnani, E. Re, P. Bologna, S. Espinasse, A. Olivieri, SD2—How to sample a comet, *Space Sci. Rev.* 128 (1–4) (2007) 281–299.
- M. Thiel, J. Stöcker, C. Rohe, N.I. Kömle, G. Kargl, O. Hillenmaier, P. Lell, The ROSETTA Lander anchoring system, 10th European Space Mechanisms and Tribology Symposium vol. 524, (2003), pp. 239–246.
- J. Biele, S. Ulamec, M. Maibaum, R. Roll, L. Witte, E. Jurado, P. Muñoz, W. Arnold, H.-U. Auster, C. Casas, et al., The landing (s) of Philae and inferences about comet surface mechanical properties, *Science* 349 (6247) (2015) aaa9816.
- K.-H. Glassmeier, H. Boehnhardt, D. Koschny, E. Kührt, I. Richter, The Rosetta mission: flying towards the origin of the solar system, *Space Sci. Rev.* 128 (1–4) (2007) 1–21.
- P. Di Lizia, F. Bernelli-Zazzera, A. Ercoli-Finzi, S. Mottola, C. Fantinati, E. Remeteau, B. Dolives, Planning and implementation of the on-comet operations of the instrument SD2 onboard the lander Philae of Rosetta mission, *Acta Astronaut.* 125 (2016) 183–195.
- W.V. Boynton, R.P. Reinert, The cryo-penetrator: an approach to exploration of icy bodies in the solar system, *Acta Astronaut.* 35 (1995) 59–68.
- R. Lorenz, W.V. Boynton, C. Turner, Demonstration of comet sample collection by penetrator, Proceedings of the 5th IAA International Conference on Low-cost Planetary Missions, 2003, pp. 387–394.
- R.D. Lorenz, Planetary penetrators: their origins, history and future, *Adv. Space Res.* 48 (3) (2011) 403–431.
- M. Badescu, R. Bonitz, A. Ganino, N. Haddad, P. Walkemeyer, P. Backes, L. Shiraishi, E. Kulczycki, N. Aisen, C.M. Dandino, et al., Dynamic Acquisition and Retrieval Tool (DART) for comet sample return, *Aerospace Conference*, 2013 IEEE, IEEE, 2013, pp. 1–12.
- J. Banik, T. Murphey, Performance Validation of the Triangular Rollable and Collapsible Mast, 24th Annual AIAA/USU Conference on Small Satellites, 2010.
- M. Daly, O. Barnouin, C. Johnson, E. Bierhaus, J. Seabrook, C. Dickinson, T. Haltigin, D. Gaudreau, C. Brunet, G. Cunningham, et al., The OSIRIS-REx laser altimeter (OLA): Development progress, Asteroids, Comets, Meteors 2014, 2014.
- D. Adams, J. Leary, S. Papadakis, C. Aplan, R. Maddock, S. Kellas, R. Winski, T. White, C. Kazemba, P. Agrawal, Comet surface sample return: Sample chain system overview, *Aerospace Conference*, 2017 IEEE, IEEE, 2017, pp. 1–7.
- G. Hirzinger, K. Landzettel, B. Brunner, M. Fischer, C. Preusche, D. Reintsema, A. Albu-Schäffer, G. Schreiber, B.-M. Steinmetz, DLR's robotics technologies for on-orbit servicing, *Adv. Robot.* 18 (2) (2004) 139–174.
- K. Landzettel, A. Albu-Schäffer, B. Brunner, A. Beyer, R. Gruber, E. Krämer, C. Preusche, D. Reintsema, J. Schott, H.J. Steinmetz, et al., ROKVISS verification of advanced light weight robotic joints and tele-presence concepts for future space missions, Proceedings of the 9th ESA Workshop on Advanced Space Technologies for Robotics and Automation, ASTRA, 2006.
- K. Landzettel, C. Preusche, A. Albu-Schäffer, D. Reintsema, B. Rebele, G. Hirzinger, Robotic on-orbit servicing—DLR's experience and perspective, *Intelligent Robots and Systems*, 2006 IEEE/RSJ International Conference on, IEEE, 2006, pp. 4587–4594.
- M.F. A'Hearn, M.J.S. Belton, W.A. Delamere, J. Kissel, K.P. Klaassen, L.A. McFadden, K.J. Meech, H.J. Melosh, P.H. Schultz, J.M. Sunshine, et al., Deep Impact: excavating comet Tempel 1, *Science* 310 (5746) (2005) 258–264.
- J.E. Richardson, H.J. Melosh, An examination of the Deep Impact collision site on Comet Tempel 1 via Stardust-NEXT: Placing further constraints on cometary surface properties, *Icarus* 222 (2) (2013) 492–501.
- O. Groussin, L. Jorda, A.-T. Auger, E. Kührt, R. Gaskell, C. Capanna, F. Scholten, F. Preusker, P. Lamy, S. Hviid, et al., Gravitational slopes, geomorphology, and material strengths of the nucleus of comet 67P/Churyumov-Gerasimenko from OSIRIS observations, *Astron. Astrophys.* 583 (2015) A32.
- E. Heggy, A. Shafie, A. Hérique, J. Lasue, W.W. Kofman, A.C. Levasseur-Regourd, Constraining the bulk Dust to Ice Ratio and Compressive Strength for Comet Churyumov Gerasimenko Using CONSERT Radar Observations, *AGU Fall Meeting Abstracts*, 2015.
- R. Roll, L. Witte, W. Arnold, ROSETTA lander Philae—soil strength analysis, *Icarus* 280 (2016) 359–365.
- T. Spohn, J. Knollenberg, A.J. Ball, M. Banaszkiwicz, J. Benkhoff, M. Grott, J. Grygorczuk, C. Hüttig, A. Hagermann, G. Kargl, et al., Thermal and mechanical properties of the near-surface layers of comet 67P/Churyumov-Gerasimenko, *Science* 349 (6247) (2015) aab0464.
- H.L. Jessberger, M. Kotthaus, J. Hunt, T.D. Guyenne (Eds.), *Compressive Strength of Synthetic Comet Nucleus Samples, Physics and Mechanics of Cometary Materials*, 1989, pp. 141–146.
- K. Seifert, T. Spohn, J. Benkhoff, Cometary ice texture and the thermal evolution of comets, *Adv. Space Res.* 15 (10) (1995) 35–38.

- [47] V. Ciarletti, A.C. Levasseur-Regourd, J. Lasue, C. Statz, D. Plettemeier, A. Hérique, Y. Rogez, W. Kofman, CONSERT suggests a change in local properties of 67P/Churyumov-Gerasimenko's nucleus at depth, *Astron. Astrophys.* 583 (2015) A40.
- [48] H. Sierks, C. Barbieri, P.L. Lamy, R. Rodrigo, D. Koschny, H. Rickman, H.U. Keller, J. Agarwal, M.F. A'Hearn, F. Angrilli, et al., On the nucleus structure and activity of comet 67P/Churyumov-Gerasimenko, *Science* 347 (6220) (2015) aaa1044.
- [49] W. Kofman, A. Hérique, Y. Barbin, J.-P. Barriot, V. Ciarletti, S. Clifford, P. Edenhofer, C. Elachi, C. Eyraud, J.-P. Goutail, et al., Properties of the 67P/Churyumov-Gerasimenko interior revealed by CONSERT radar, *Science* 349 (6247) (2015) aab0639.
- [50] Pittsburgh Corning Corporation, FOAMGLASS® Insulation Datasheets, (2018) <https://industry.foamglas.com/en-gb/resources/datasheets>.
- [51] ASTM International, West Conshohocken, PA, ASTM C165-07(2017), Standard Test Method for Measuring Compressive Properties of Thermal Insulations, (2017) <https://www.astm.org/>.
- [52] E.M. Carey, G.H. Peters, M. Choukroun, L. Chu, E. Carpenter, L. Panossian, Y.M. Zhou, A. Sarkissian, S. Moreland, L.R. Shiraishi, et al., Comparison of the Mechanical Porous Ambient Comet Simulants (MPACS) to Other Comet Surface Analog Materials, Lunar and Planetary Science Conference vol. 48, (2017).
- [53] J. Biele, S. Ulamec, L. Richter, J. Knollenberg, E. Kühr, D. Möhlmann, The putative mechanical strength of comet surface material applied to landing on a comet, *Acta Astronaut.* 65 (7) (2009) 1168–1178.
- [54] S. Ulamec, C. Fantinati, M. Maibaum, K. Geurts, J. Biele, S. Jansen, O. Küchemann, B. Cozzoni, F. Finke, V. Lommatsch, et al., Rosetta lander-landing and operations on comet 67P/Churyumov-Gerasimenko, *Acta Astronaut.* 125 (2016) 80–91.
- [55] J. Corner, A theory of the internal ballistics of the "Hoch-und-Niederdruck Kanone", *J. Franklin Inst.* 246 (3) (1948) 233–248.
- [56] G. Backstein, et al., *Handbook on Weaponry*, Rheinmetall GmbH, Düsseldorf, 1982.
- [57] J.E. Pleasants, Parachute Mortar Design, *J. Spacecraft Rockets* 11 (4) (1974) 246–251.
- [58] R.E. Vasas, J. Styner, Mars Exploration Rover Parachute Mortar Deployer Development, In: *17th AIAA Aerodynamic Decelerator Systems Technology Conference and Seminar*, p. 2137, (2003).
- [59] B.W. Rosen, *Mechanics of composite strengthening*, Fiber Composite Materials, American Society of Metals, 1965, pp. 37–75 Ch. 3.
- [60] N.A. Fleck, *Compressive failure of fiber composites*, *Advances in Applied Mechanics*, vol. 33, Academic Press, New York, NY, 1997, pp. 43–117.
- [61] L.R. Purves, J.A. Nuth, E. Amatucci, Video Supplement: Development and Testing of Harpoon-Based Approaches for Collecting Comet Samples, (2017) <https://ntrs.nasa.gov/archive/nasa/casi.ntrs.nasa.gov/20170004092.pdf> NASA/TM-2017-219018/Supplement.
- [62] P. Fritzson, V. Engelson, Modelica - A unified object-oriented language for system modeling and simulation, *European Conference on Object-oriented Programming*, Springer, 1998, pp. 67–90.
- [63] P. Fritzson, *Principles of Object-oriented Modeling and Simulation with Modelica 3.3: a Cyber-physical Approach*, John Wiley & Sons, 2014.
- [64] C. Andersson, C. Führer, J. Åkesson, Assimulo: A unified framework for ODE solvers, *Math. Comput. Simulat.* 116 (2015) 26–43.
- [65] J. Corner, *Theory of the interior Ballistics of Guns*, John Wiley and Sons Inc., New York, 1950.
- [66] D.E. Carlucci, S.S. Jacobson, *Ballistics: Theory and Design of Guns and Ammunition*, CRC Press, 2013.
- [67] M.S. Miller, *Burning-Rate Models and Their Successors, a Personal Perspective, Overviews of Recent Research on Energetic Materials*, World Scientific, 2005, pp. 419–472.
- [68] S. Gordon, B.J. MacBride, *Computer Program for Calculation of Complex Chemical Equilibrium Compositions and Applications*, NASA Reference Publication 1 & 2, NASA, (October 1994).
- [69] H. Dubbel, B.J. Davies, *Dubbel-Handbook of Mechanical Engineering*, Springer Science & Business Media, 2013.
- [70] M.M. Abbott, H.C. Van Ness, *Schaum's Outline of Theory and Problems of Thermodynamics*, McGraw-Hill, 1972.